Slow Relaxations of Hydration Water near a Lipid Membrane: a Molecular Dynamics Study

A Thesis submitted by

Abhinav Srivastava

in partial fulfillment of the requirements for the award of the degree of

Doctor of Philosophy

Indian Institute of Technology Jodhpur
Department of Chemistry

September 2020

5

Dynamic coupling of hydration water near a phospholipid membrane

5.1 INTRODUCTION

Biological water near lipid membranes has received a lot of attention since hydration sites of lipid membranes and hydrogen bonded network of hydration water are found to be crucial for understanding membrane-membrane interactions [Brzustowicz and Brunger, 2005; de Vries *et al.*, 2005; Polak *et al.*, 2014; Kučerka *et al.*, 2015; Fogarty *et al.*, 2015; Andoh *et al.*, 2016; Lin *et al.*, 2018]. To establish a relation between membrane and hydration layer dynamics and its connection to membrane functionalities, membrane associated protein-water dynamics have been analyzed where a correlation has been found to persist till 2.5 nm between two biosurfaces [Päslack *et al.*, 2019a]. 1H Overhauser dynamic nuclear polarization enhanced NMR relaxometry experiments show that dynamics of water near a membrane can be used as a predictor of membrane associated protein topology, structure, immersion depth [Cheng *et al.*, 2013]. Hydration water forms stronger hydrogen bonded networks with the phosphate group of lipid heads rather than other lipid head moieties [Re *et al.*, 2014]. All atom molecular dynamics simulations show that thermodynamical and dynamical properties of interface water near a bilayer follow a transition near the phase transition temperature of bilayers [Debnath *et al.*, 2013]. Molecular dynamics simulations and Overhauser DNP-enhanced NMR experiments show that water dynamics is strongly slowed down near the electrostatic interface of membrane-water and at larger distances away from the interface, it is dominated by the protein [Fisette *et al.*, 2016]. Distance dependency of hydration dynamics at the membrane interface has been investigated using molecular dynamics simulations revealing cooperative motion of water and lipid molecules [Das *et al.*, 2013]. Sum frequency generation spectroscopy and ab-initio molecular dynamics simulations show that continuous hydrogen bonded network can be formed from the bulk water to the carbonyl group of lipid molecules [Ohto *et al.*, 2015]. Correlated motions of water and protein and membrane have been identified in purple membranes [Tobias *et al.*, 2009]. Correlated motion of lipid molecules occurs over 3 nm which can consist of 4 lipid molecules with a time span from ps to close to ten ns [Rheinstädter *et al.*, 2008].

Similar to the hydration layers near membranes, coupled protein-water motions are observed over tens of ps for the slow relaxations [Li *et al.*, 2007]. Regional structure and dynamics of interface water near a protein are sensitive to the topological heterogeneity of the protein surface rather than to the chemical specificity of the protein structure [Dahanayake and Mitchell-Koch, 2018a]. Earlier experiments with limited energy resolutions of ~ 1 μev have prompted researchers to the idea of perfect coupling of protein dynamical transition (PDT) to the hydration water relaxation dynamics [Doster *et al.*, 1989; Chen *et al.*, 2006; Schiró *et al.*, 2015]. However, on the contrary, protein dynamical cross-overs have been reported at a temperature different from PDT or even at a dry state [Liu *et al.*, 2017]. Recent high resolution elastic neutron scattering experiment shows decoupling between protein and hydration water dynamics at low temperature [Benedetto, 2017]. This imposes serious questions on the well established thought of a perfect coupling between protein and hydration water.

At supercooled temperatures ranging from 100 K to 260 K, dynamic coupling between hydration water and membrane is no longer valid. For temperatures <260 K, membrane protein dynamics is not controlled by hydration water, rather, it is controlled by the dynamics of lipid [Wood *et al.*, 2007]. Similar to the protein-water coupling, it is not clear if the influence of water dynamics on membrane dynamics is significant enough to control the function of the membrane. If it is not significant,

what makes water dynamics a good predictor of membrane structure and topology is a topic of active research. The atomistic details of dynamic coupling between chemically confined hydration water and lipid interaction sites are still remain inconclusive. Controlling factors of heterogeneous distributions of hydration water near membrane surfaces leading to dynamical heterogeneities are not clearly understood.

Thus, in this chapter, we attempt to understand the coupling of hydration water and membrane dynamics by probing the membrane behavior from the hydrophobic core towards the hydrophilic region employing all atom molecular dynamics simulations. We calculate two dimensional mean square displacements, one dimensional van Hove Correlation functions of lipid components and interface water molecules on the membrane surface. van Hove correlation functions examine the presence of dynamical heterogeneity in both water molecules and the lipid bilayer at fluid phase. Earlier simulations have shown that lipid molecules exhibit dynamical heterogeneity in a membrane at L_β phase due to the presence of different mobility groups [Shafique *et al.*, 2016]. Dynamical heterogeneities have been observed in a binary lipid cholesterol membrane and even in a fluid membrane in absence of cholesterol on the scale of $80 - 150$ nm [Sarangi *et al.*, 2017; Roobala and K., 2017]. However, these results do not provide the correlations between local dynamics of membrane and the neighboring water dynamics contributing towards dynamical heterogeneity. To understand the origin of dynamical heterogeneity in the interface water under the influence of lipid molecules, we calculate probability distribution of logarithm of translational displacements. The probability distributions are calculated for different times for both lipids and water molecules to check the presence of a bimodal behavior. The bimodal behavior manifests intermittent dynamics in solute motion and can play a dominant role on Fickian and non-Gaussian behavior [Acharya *et al.*, 2017]. Colloidal systems are found to exhibit similar dynamics in crowded environments [Kwon *et al.*, 2014]. Representative trajectories of an interface water and a lipid molecule are plotted showing the presence of translational jump from one hydrogen bonded lipid partner to the other. Two dimensional self intermediate scattering functions are calculated for both lipid and interface water molecules on the bilayer surface. Multiple relaxation time scales present in the lipid molecules and the interface water are quantified. Correlations between relaxation times of lipid and interface water molecules are analyzed. These systematic analyses highlight the role of lipid moieties on the coupling or decoupling of interface water relaxations at multiple time-scales. Our results enhance the fundamental understanding on the influence of membrane dynamics on hydration layer dynamics which have future implications on sensing membrane functions due to external perturbations or chemical binding.

5.2 SIMULATION DETAILS

All atom molecular dynamics simulations are carried out for 128 DMPC lipid molecules fully hydrated with 5743 TIP4P/2005 [Abascal and Vega, 2005] water molecules. Thus ~ 45 water molecules per lipid are present which suffice the hydration number for DMPC as reported earlier in experiments [Lopez *et al.*, 2004; Zhao *et al.*, 2008; Trapp *et al.*, 2010]. DMPC force field parameters are obtained using Berger united atom force fields [Berger *et al.*, 1997; Cordomí *et al.*, 2012]. Berger force fields in combination with TIP4P/2005 water model is found to be suitable in calculating heterogeneity in the structure and dynamics of water near a membrane [Srivastava *et al.*, 2019b]. An NPT simulation is carried out for 100 ns with a 2 fs time step and 200 ps saving frequency. The bilayer is equilibrated at 308 K temperature using velocity rescaling method [Bussi *et al.*, 2007] with a 0.5 ps coupling constant. Pressure of 1 bar is maintained using Berendsen pressure coupling method [Berendsen *et al.*, 1984b] with a 0.1 ps coupling constant and compressibility of 4.5×10^{-5} bar^{-1}. van der Waals interactions are cutoff at 1 nm. Particle mesh Ewald method [Allen and Tildesley, 1987; Darden *et al.*, 1993; Essmann *et al.*, 1995b] is applied with a 0.12 nm grid size for corrections in long range interactions. Periodic boundary conditions are applied in all three directions. Bonds are kept constant using LINCS [Hess *et al.*, 1997] algorithm. Next, an NVT run

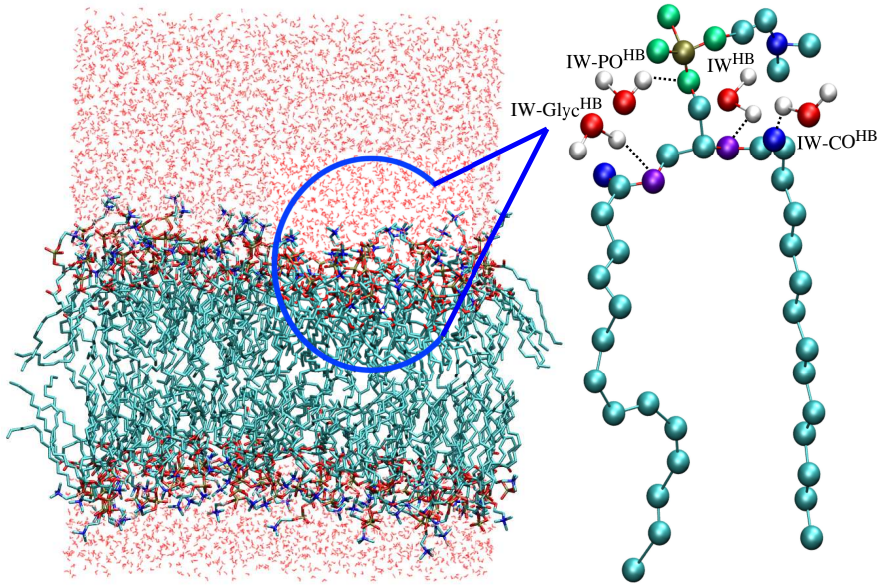

Figure 5.1: Snapshot of a hydrated DMPC bilayer and a DMPC molecule in presence of IW^{HB} molecules hydrogen bonded to lipid moieties residing near N head-groups.

is carried out for 20 ns with a 0.4 fs time step and a 10 fs saving frequency. Temperature and pressure coupling parameters, long and short range distance corrections are kept same for the NPT run. Box lengths of the bilayer are 6.24 nm in x and y and 7.95 nm in z direction. 10 sets of uncorrelated runs each with 1 ns run-length is used for the calculations of water dynamics. Each result is obtained by averaging over 10 uncorrelated blocks of data each with $10,000$ frames using in-house codes.
We also simulate bulk water (BW) using TIP4P/2005 water model consisting of 851 water molecules at 308 K temperature as discussed in the previous chapter. All simulations are performed with GROMACS-4.6.5 [Bekker *et al.*, 1993; Berendsen *et al.*, 1995; Lindahl *et al.*, 2001; Spoel *et al.*, 2005; Hess *et al.*, 2008] software package.

5.3 MEMBRANE DYNAMICS

For probing membrane dynamics, different lipid moieties are identified based on hydrophilic and hydrophobic characteristics exhibited by the lipids. The head-group hydrophilic moieties are N_{Head} (nitrogen), $Carb_{Head}$ (carbonyl carbons), $Glyc_{Head}$ (glycerol carbons) and P_{Head} (phosphorus). Hydrophobic alkyl chains are referred to as $B1_{Tail}$, $B2_{Tail}$ and $B3_{Tail}$. A snapshot of DMPC beads is shown in figure 5.2. For calculating dynamical properties, center of mass of same moiety from two hydrophobic alkyl chains of a DMPC molecule is considered. Interface water molecules are identified based on the geometric criteria of their proximity of ± 0.3 nm from the nitrogen head-group of DMPC and referred to as IW^{HB}. If a IW^{HB} is hydrogen bonded to phosphate or carbonyl or glycerol oxygens for even a single time frame during its confinement time, the molecule is referred to as IW-PO^{HB}, IW-CO^{HB} and IW-Glyc^{HB} respectively. these are identified in a similar way as mentioned in chapter 3, section 3.3. Density profiles for all classes of IW^{HB} exhibit restrained behavior near N head-group of DMPC for 100 ps confinement lifetime (figure 5.3 a)). The density profiles of IW^{HB} indicate that IW-PO^{HB}, IW-CO^{HB}, IW-Glyc^{HB} form hydrogen bonds to P, Carb and Glyc oxygens by residing close to the Nitrogen head-group density as they do not change their locations near the HB partners. Less associations of all classes of IW^{HB} near hydrophilic region are observed for 1 ns while more association of water near the head was found

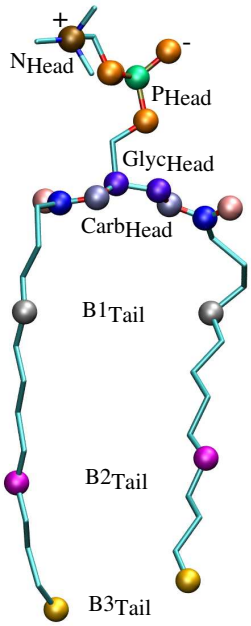

Figure 5.2: Hydrophilic and hydrophobic beads of a DMPC molecule for which dynamical calculations are performed. Color codes: VDW Ochre - Nitrogen (N_{Head}), Green - Phosphorus (P_{Head}), Orange - Oxygen atoms associated with phosphate group, Pink - Oxygen atoms of carbonyl moiety, Ice blue - Oxygen atoms of glycerol moiety, Violet - Carbon atoms of glycerol moiety ($Glyc_{Head}$), Blue - Carbon atoms of carbonyl moiety ($Carb_{Head}$), Silver - $B1_{Tail}$, Magenta - $B2_{tail}$ and Orange - $B3_{Tail}$.

for 100 ps. The molecules tend to diffuse into the bulk region from the hydrophilic head group regime when the density profiles are calculated for 1 ns (figure 5.3 b))

5.4 TRANSLATIONAL MEAN SQUARE DISPLACEMENT

For quantifying translational dynamics, we first calculate 2D translational mean square displacements (MSD_{XY}) of IW^{HB} and DMPC beads using equation 2.1. Figure 5.4 shows translational mean square displacement (MSD_{XY}) on the bilayer XY surface for DMPC beads and IW^{HB}. Bulk water molecules (BW) reach diffusive regime much faster ($\sim$ 10 ps) than that of IW^{HB}. IW^{HB} molecules enter into the diffusive regime with a diffusion exponent of $\sim$ 0.98 (figure 5.4) at $\sim$ 80 ps which is close to its confinement lifetime. They enter in the sub-diffusive regime within $\sim 5 - 10$ ps. (table 5.1). The lipid components reach similar values of MSD_{XY} at much later time $\sim 100 - 300$ ps (table 5.2). Interestingly, MSD_{XY} of lipid components increase from head-groups to tail (figure 5.4). $B3_{Tail}$ has the highest MSD_{XY} among all components of lipids although $B3_{Tail}$ situates at the midplane of the hydrophobic bilayer. This signifies that the translational motion of the end beads of the hydrophobic tails are faster than the heads since the alkyl tails are not hydrogen bonded. The behavior of MSD_{XY} of carbon and oxygens of Carb/Glyc and P and oxygens of PO show very similar sub-diffusive trends. MSD_{XY} of carbon and oxygen atoms of same moieties are calculated to check the effect of mass on MSD_{XY}. The MSD_{XY} of Glyc is slowest among all components of lipids. MSD_{XY} of IW^{HB} have been shown in figure 5.5. IW^{HB} do not show any significant difference in MSD_{XY} when identified based on their hydrogen bond partners such as IW-PO^{HB}, IW-CO^{HB} and IW-$Glyc^{HB}$ (inset in figure 5.5).
For gaining deeper insights on translational mobility of hydrogen bonded interfacial waters, retardation factor (RF) is calculated for all DMPC beads as well as for all classes of IW^{HB} which are

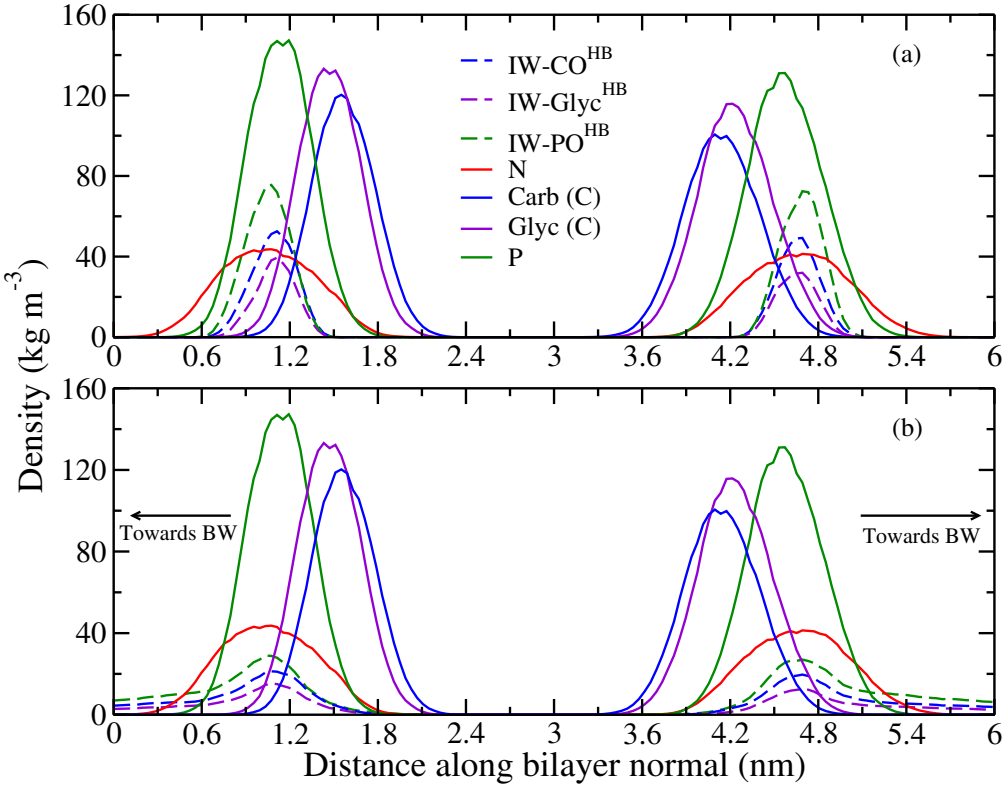

Figure 5.3: Density profiles of DMPC lipids and all classes of IW^{HB} along the bilayer normal. Density profiles of all classes of IW^{HB} are averaged over a) 100 ps and b) 1 ns.

averaged over 10 sets of uncorrelated data each of 1 ns run length. Retardation factor measures the slow down in mobility of solute with respect to the solvent [Abseher *et al.*, 1996; Franck *et al.*, 2015; Braun *et al.*, 2016; Barnes *et al.*, 2017; Dahanayake and Mitchell-Koch, 2018b]. RF is calculated as $\frac{MSD_{XY}(BW)}{MSD_{XY}(Lipid)}$ for DMPC and $\frac{MSD_{XY}(BW)}{MSD_{XY}(IW)}$ for IW^{HB}. For $MSD_{XY}(Lipid)$, COM of lipid is considered for MSD calculation. Figure 5.6 a) shows that Glyc. moiety of lipids have maximum RF followed by a decrease in RF as moving from P to N moieties of the lipid heads. This confirms a lowering in retardation of lipid moieties facing the outer most water regime. However, RF for all classes of IW^{HB} do not differ significantly as all of these IW^{HB} are confined near the N head-group and then form hydrogen bonds to the other lipid moieties. Ratio of retardation factors of lipids with respect to IW^{HB} are shown in figure 5.6 b). Glyc moiety buried deep in the hydrophobic core of the lipid show maximum retardation with respect to the IW-$Glyc^{HB}$ molecules. Since RF of different classes of IW^{HB} do not differ much, the ratio of RF of lipid to IW^{HB} follow similar trend as the RF of lipids.

5.5 TRANSLATIONAL VAN HOVE CORRELATION

For investigating heterogeneous dynamics on the bilayer surface, self part of one dimensional (1D) van Hove correlation function is calculated for all classes of IW^{HB} corresponding to time scales mentioned in table 5.1. Similarly, 1D van Hove correlation functions of DMPC are calculated for a time scale mentioned in table 5.2. It is to be noted that at these time scales, all classes of IW^{HB} and lipid moieties are still in sub-diffusive regime as mentioned in figure 5.5. Tails of lipids viz. $B1_{Tail}$, $B2_{Tail}$ and $B3_{Tail}$ deviate minimum from Gaussianity while maximum deviations from Gaussianity are observed for lipid heads (figure 5.7). On approaching the lipid-water from the hydrophobic core of lipids, deviations from Gaussianity are found to decrease (figure 5.8). Emergence of

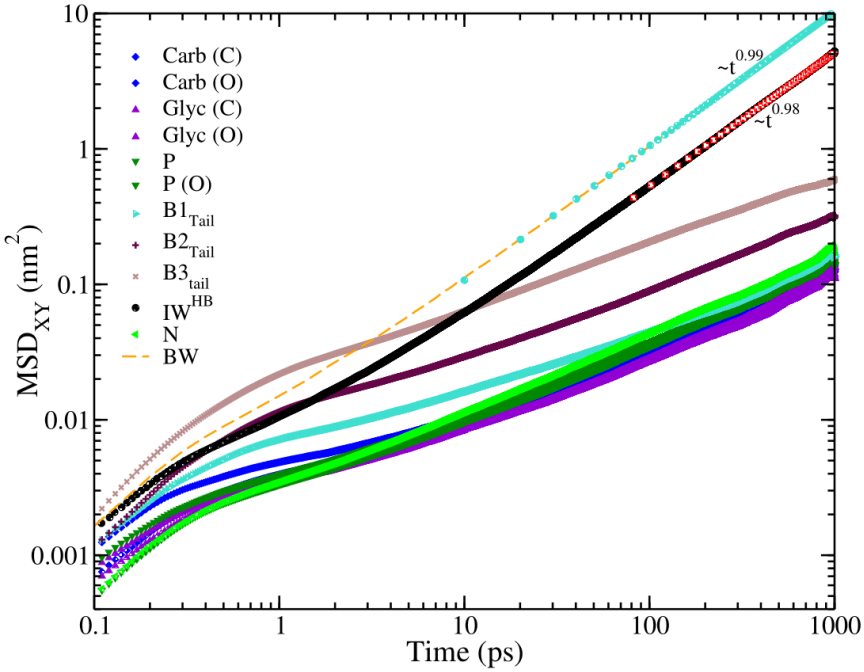

Figure 5.4: Two dimensional translational mean square displacement (MSD_{XY}) of all beads of DMPC, IW^{HB} and BW.

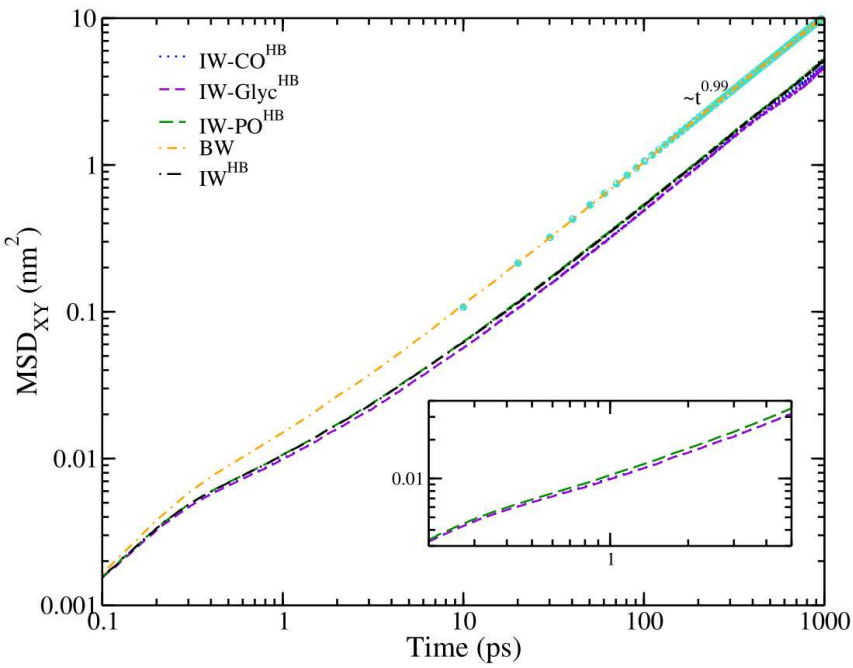

Figure 5.5: Two dimensional translational mean square displacement (MSD_{XY}) of all classes of IW^{HB} and BW. Inset: different classes of IW^{HB} show similar MSD_{XY}.

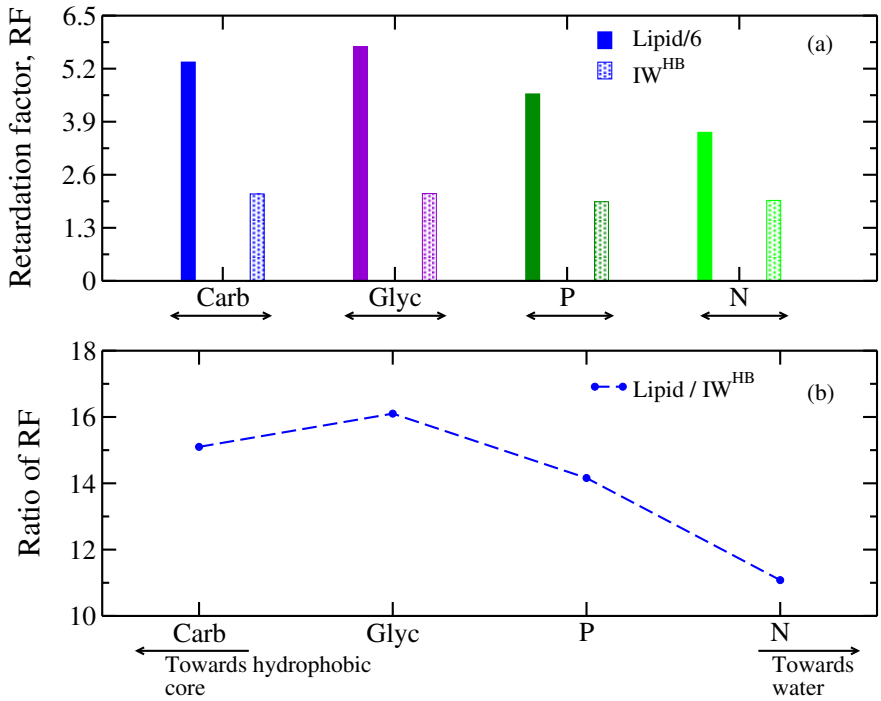

Figure 5.6: a) Retardation factor calculated for DMPC lipid moieties and IW^{HB} with respect to BW. Glyc beads show maximum retardation due to its buried nature in hydrophobic core. b) Ratio of RF showing retardation of lipids with respect to IW^{HB}. The ratio is maximum for Glyc moiety followed by a decrease from Carb to P to N.

non-Gaussianity in one dimensional van Hove correlation function is a universal feature of dynamical heterogeneity [Hove, 1954; Kegel and van Blaaderen, 2000; Puertas *et al.*, 2004; Chaudhuri *et al.*, 2007; Sengupta and Karmakar, 2014; Jaiswal *et al.*, 2015]. The heterogeneous behavior of IW^{HB} is due to their chemically confined nature. Non-Gaussianity in van Hove correlation function of lipid beads decreases as moving towards hydrophobic alkyl chains of the DMPC. $B3_{Tail}$ and N bead of the DMPC manifest least and strong deviations from Gaussianity respectively (figure 5.7). The maximum deviations of IW^{HB} hydrogen bonded to Glyc closer to the deep hydrophobic core and less deviations of lipid Glyc. components from Gaussianity with sub-diffusive dynamics are puzzling and contradictory at the first glance. According to the law of Brownian motion, a solute particle moving through a medium follows the theory of random walk. If the solute particle follows Fickian or diffusive behavior, the probability displacements of the particles should be Gaussian in nature [Einstein, 1906]. However recent report shows that particles with diffusing diffusivity in a crowded medium can have Fickian diffusion with non-Gaussian probability distributions in displacements [Jain and Sebastian, 2016]. So Fickian MSD_{XY} with prominent non-Gaussianity in G_s(x,t) of IW^{HB} and sub-linearity in MSD_{XY} with less non-Gaussian G_s(x,t) in lipid components need special attention and further analysis. These features confirm that MSD_{XY} is not a good measure to understand the laws of Brownian motion originally derived for motion of a solute through a medium. To understand the underlying phenomenon, $P(log_{10}(r(t))) = 4\pi r^3 ln(10) G_s(r,t)$ is calculated and shown in figure 5.9. For bulk water, the value of the most probable distribution of $P(\log_{10}r(t)) \approx 2.13$ at time 45 ps. This clearly indicates that the BW molecules follow Gaussian distributions with Fickian dynamics. A departure from the value 2.13 indicates deviations from Gaussianity [Acharya *et al.*, 2017]. The value of the distribution for the IW^{HB} is much lower than 2.13 with highly non-Gaussian probability distribution at 5.12 ps because the IW^{HB} molecules are at sub-diffusive regime at that time. At a later time of 78.7 ps, IW^{HB} molecules reach the linear behavior in MSD_{XY}, but have a very distinct bi-modal nature characterizing intermittency in dynamics of IW^{HB}. Similar intermittent dynamics is common in supercooled liquids due to

domain formation. In the case of IW^{HB}, there is no domain formation, but IW^{HB} molecules are still stuck at a transient cage formed by the lipid head-groups for some time and then hop or jump from there to another transient cage leading to intermittency in dynamics. At a much longer time (at 154) ps which is ~ 4 times the value of diffusive time, the bi-modal nature still persists. At 610 ps, the peak of $P(\log_{10}r(t))$ of IW^{HB} shifts to the right hand side in figure 5.9. Although the bimodal nature is not retained, the peak value is much lower than 2.13. The time evolution of $P(\log_{10}r(t))$ of IW^{HB} does not lead to Gaussian behavior even at ~ 7.7 times of diffusive limiting time. The probability distribution is calculated for a lipid head (P) to check the correlation between membrane and IW^{HB} dynamics. Time evolution of $P(\log_{10}r(t))$ of P lipid head does not show much changes in their behavior within 200 ps indicating very slow dynamics of P lipid heads compared to the IW^{HB}. The peak value of $P(\log_{10}r(t))$ of the lipid is close to 2.13 and consistent with less deviations from Gaussianity in their $G_s(x,t)$. The less deviations from Gaussianity probably originate from their vibrations in the cage formed by the neighboring lipid heads. The time evolution of $P(\log_{10}r(t))$ for both IW^{HB} and lipid head P, clearly demonstrate the presence of intermittency in IW^{HB} dynamics and the absence of perfect coupling in lipid and IW^{HB} dynamics via same relaxation time scales throughout the entire observation time period.

The intermittency in dynamics of IW^{HB} and the imperfect coupling of lipids and IW^{HB} are clearly observed when a trajectory of a single IW^{HB} molecule is plotted and shown in figure 5.10. The trajectories of single IW^{HB} molecule and two lipid head-groups, viz. Carb and P are shown. The trajectories of the IW^{HB}, Carb, and P of lipids are shown in black, blue and green respectively. The trajectory of the IW^{HB} molecule shows the presence of three sticky segments S1, S2 and S3. The IW^{HB} molecule transiently spends some time in each sticky segment followed by a translational jump from one segment to another. This is a clear manifestation of intermittency in dynamics of IW^{HB}. The IW^{HB} molecule is hydrogen bonded to the carbonyl (Carb) oxygen of a lipid molecule while residing in the segment S1 as shown in figure 5.10. After it resides in the transient cage of S1, it jumps from S1 to S2 and form a hydrogen bond to the P oxygen of another lipid molecule and reside in that transient cage S2. After some time, the IW^{HB} molecule again jumps from segment S2 to S3. Similar translational jump has been found to be the origin of decoupling between translational diffusion and viscosity in supercooled bulk water molecules [Dueby *et al.*, 2019]. While the IW^{HB} molecule jumps from S1 to S2 to S3 after residing at each segment or cage for a small duration, the hydrogen bonded lipid partners do not move or jump coherently with the IW^{HB} molecule. Instead they remain stationary near the respective segments for more time and then move after a time lag. This clearly shows that the IW^{HB} and the lipid molecules in the membrane do not obey the concept of perfect coupling. Perfect coupling exists if the relaxation dynamics of two or more processes are occurring on the same time scale. For instance, in proteins, fluctuations in the bulk water are coupled with large scale motion of proteins. The internal motion of proteins are coupled with β-relaxations of the hydration water [Frauenfelder *et al.*, 2009]. Similarly, for membranes, hydration water dynamics and membrane dynamics should be of the same order. However, it is reported that lower temperatures, the concept of perfect coupling no longer holds valid and hydration water dynamics and membrane/protein dynamics are decoupled [Wood *et al.*, 2007; Benedetto, 2017]. The coupling between IW^{HB} and lipids occur with some scaling factor which is discussed later.

Table 5.1: Time of entrance to the sub-diffusive regime for different classes of IW^{HB} as obtained from 10 sets of MSD_{XY}.

Beads	Δt_1 (ps)	Δt_2 (ps)	Δt_3 (ps)	Δt_4 (ps)	Δt_5 (ps)	Δt_6 (ps)	Δt_7 (ps)	Δt_8 (ps)	Δt_9 (ps)	Δt_{10} (ps)
IW^{HB}	6.07	5.11	5.75	6.51	5.02	5.08	7.86	5.51	6.58	5.37
IW-CO^{HB}	6.94	5.93	6.22	7.06	5.71	5.56	8.56	5.68	6.70	6.03
IW-$Glyc^{HB}$	6.26	5.22	6.05	8.11	5.60	5.89	10.70	5.87	6.74	6.11
IW-PO^{HB}	6.14	5.06	5.74	6.46	3.73	5.10	7.44	5.45	6.34	5.31

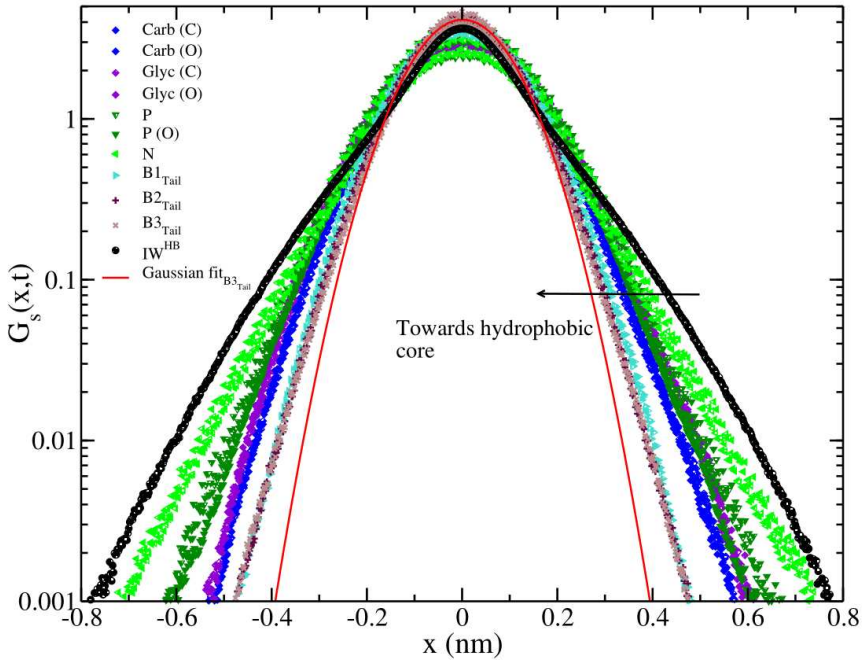

Figure 5.7: One dimensional van Hove correlation function of DMPC beads and IW^{HB}. End beads of lipid tails have minimum deviations from Gaussianity.

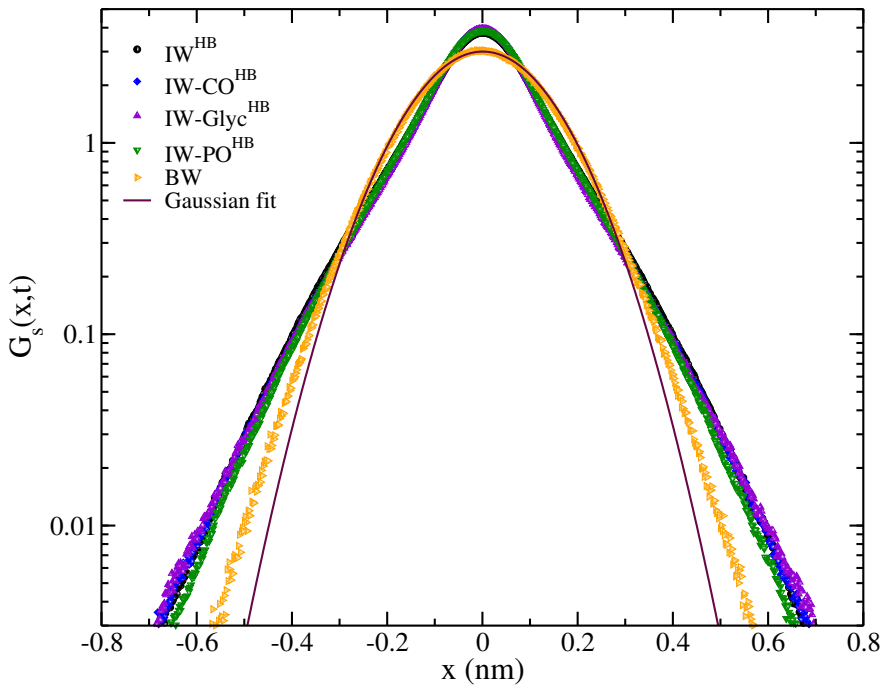

Figure 5.8: One dimensional van Hove correlation function of all classes of IW^{HB}. IW-PO^{HB} close to the lipid-water interface have minimum deviations from Gaussianity.

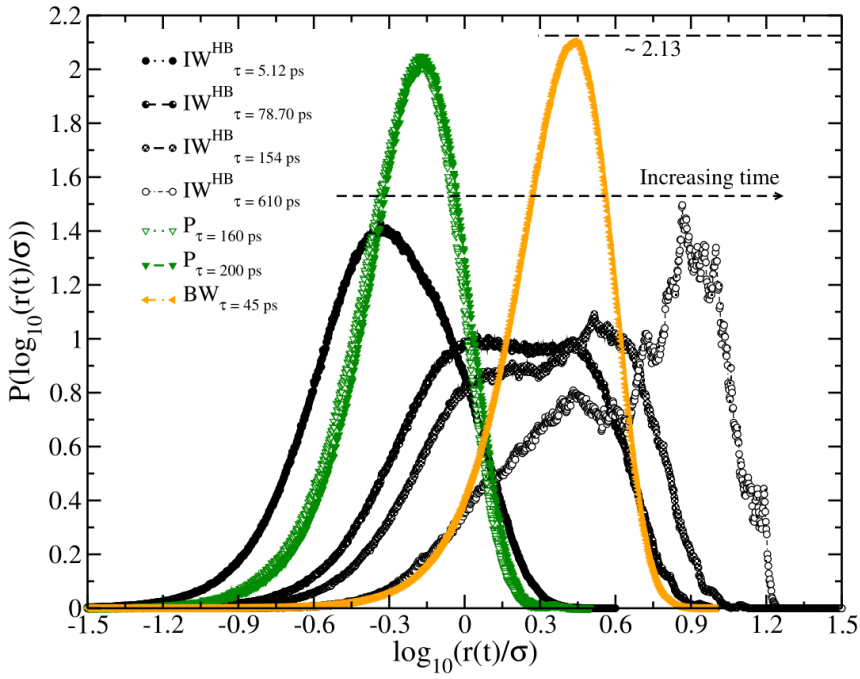

Figure 5.9: Time evolution of P ($\log_{10}(r(t)/\sigma)$) of IW^{HB}, P (phosphate) and BW. The peak of BW at ~ 2.13 corresponds to Gaussianity. IW^{HB} molecules reveal a bimodal nature characterizing presence of intermittency at a time scale when Fickian dynamics is followed.

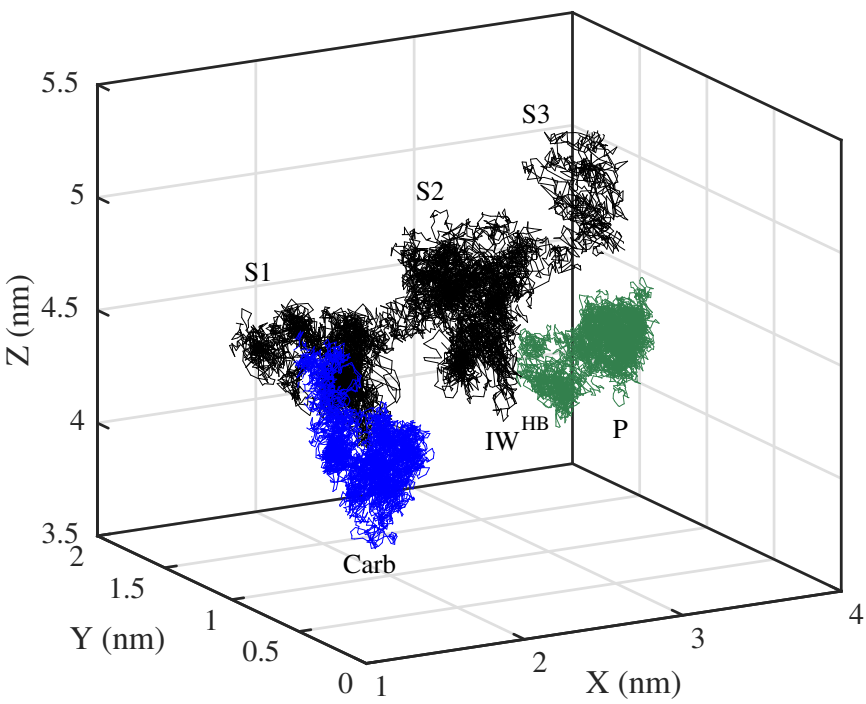

Figure 5.10: Trajectory of an atom of IW^{HB}, carbonyl carbon (Carb) and phosphorus (P) for 1 ns run length. S1, S2 and S3 represent three segments of the IW^{HB} trajectory showing three regions with consequent hopping from one region to the other. IW^{HB} remains hydrogen bonded to oxygens of Carb and P in these regions.

Table 5.2: Time of entrance to the sub-diffusive regime of DMPC beads as obtained from average of 10 sets of MSD_{XY}.

Beads	Δ t (ps)
Carb $(C)_{Head}$	156.32 ± 37.64
Carb $(O)_{Head}$	160.56 ± 27.58
Glyc $(C)_{Head}$	201.40 ± 57.56
Glyc $(O)_{Head}$	201.50 ± 40.76
P_{Head}	131.90 ± 29.47
P $(O)_{Head}$	119.67 ± 15.35
N_{Head}	81.34 ± 6.19
$B1_{Tail}$	79.33 ± 7.07
$B2_{Tail}$	18.99 ± 0.47
$B3_{Tail}$	2.93 ± 0.09

5.6 SELF INTERMEDIATE SCATTERING FUNCTION

Self intermediate scattering function (SISF) is another universal feature characterizing dynamical heterogeneities. Two dimensional SISF on the bilayer surface is calculated by equation 1.2. For quantifying membrane and IW heterogeneity, SISF are calculated for all moieties of DMPC lipids and IW^{HB} at $\lambda = 0.60$ nm for a run-length of 10 ns (figure 5.11). As the first peaks of g(r) are at ~ 0.3 nm and 0.9 nm for $IW^{HB}$and N head of DMPC respectively, an intermediate wavelength, $\lambda = 0.60$ nm, is chosen to calculate SISF. Tails (B1, B2, B3) of the lipids relax faster than the head-groups (Carb, Glyc, P) of the lipids. Since there are no IW^{HB} in the midplane of the bilayer, tails of the lipids get free space for flexible motion and at the same time no hydrogen bonds can restrict their motion. SISF of carbon oxygen and phosphorus oxygen of the same moiety show similar behavior. SISF of lipid moieties are fitted with Kohlrausch-William-Watt (KWW) function (4.1). The fitted parameters, f_Q, τ_s, τ_α, β_α are listed in table 5.3. SISF of IW-CO/PO/Glyc hydrogen bonded to different moieties of lipid head groups are shown in figure 5.12 after averaging over 10 blocks of data sets each with a run-length of 1 ns. In compared with the BW, all IW^{HB} relax much slower where IW-CO^{HB}/$Glyc^{HB}$ buried most in the hydrophobic core relax slowest. F_s(q,t) of IW-PO^{HB} and IW-CO^{HB}/$Glyc^{HB}$ show small differences in relaxations. However, SISF of IW^{HB} are not fit to the KWW function due to the appearance of long time tails τ_l. Similar long time tail has been identified earlier for interface water molecules near proteins and lipids [Marzio *et al.*, 2016; Srivastava *et al.*, 2019a]. F_s(q,t) of IW^{HB} are fitted with equation 4.2. The fitted parameters are mentioned in Table 5.4.

5.7 CORRELATIONS IN LIPID AND IW DYNAMICS

In order to understand the coupling between IW^{HB} and lipid relaxations, τ_s of both lipids and IW^{HB} are plotted in figure 5.13 a). τ_s of lipids decrease from Carb to Glyc to P to N as N is the outermost head group facing bulk water and thus is most mobile. However, τ_s of IW^{HB} does not follow similar trend as moving from inner core towards the outer surface. Note, that the values of τ_s are in the sub-ps range and therefore the differences in τ_s between various classes of IW^{HB} are also very small. To measure the extent of coupling between the fast relaxations of lipids and IW^{HB}, $\frac{\tau_s(lipid)}{\tau_s(IW)}$ is plotted in figure 5.13 b). For all classes of IW^{HB}, the ratios decrease from Carb to Glyc to P to N and the ratio is ~ 1.1 for N. This suggests that the fast relaxations of all classes of IW^{HB} and respective lipid moieties occur at very similar time scale. The fastest relaxations are strongly coupled because both IW^{HB} and respective lipid moieties vibrate in the local cage formed by the nearest neighbors and regionally relax together.

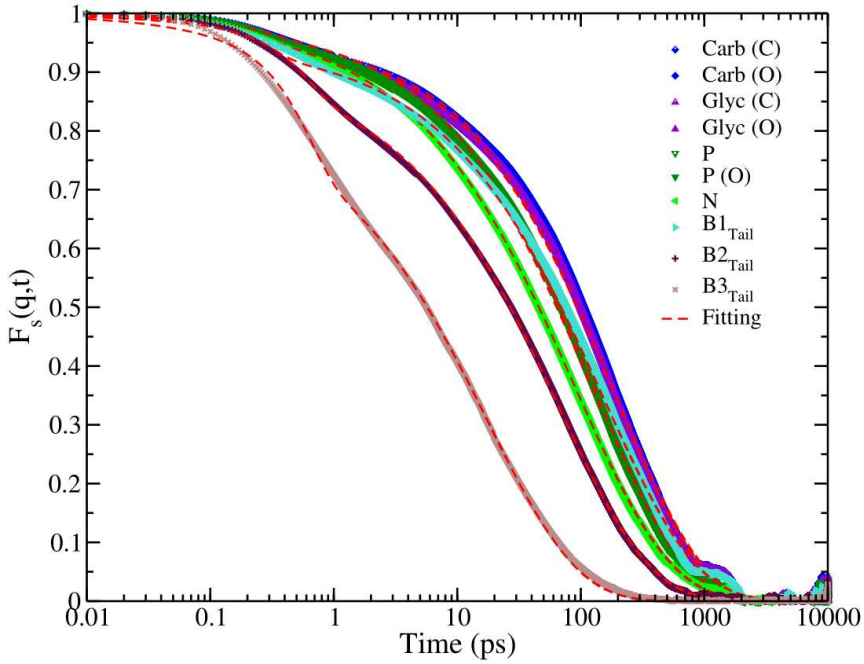

Figure 5.11: SISF of different beads of DMPC lipids for $\lambda = 0.60$ nm. Two ends of a lipid chain relax faster compared to the moieties situated in the middle.

Table 5.3: Fitted parameters of SISF of different moieties of DMPC molecule for $\lambda = 0.60$ nm along the chain. All correlation coefficients are >0.99.

Region	τ_s (ps)	f_Q	τ_α (ps)	β_α
N $_{\text{Head}}$	0.29	0.97	91.65	0.57
P $_{\text{Head}}$	0.31	0.98	124.75	0.60
P (O)$_{\text{Head}}$	0.31	0.98	129.35	0.60
Carb (C)$_{\text{Head}}$	0.40	0.96	197.32	0.63
Carb (O)$_{\text{Head}}$	0.40	0.95	189.06	0.63
Glyc (C)$_{\text{Head}}$	0.33	0.97	179.91	0.62
Glyc (O)$_{\text{Head}}$	0.33	0.96	186.33	0.62
B1$_{\text{Tail}}$	0.37	0.95	150.94	0.58
B2$_{\text{Tail}}$	0.71	0.90	66.89	0.59
B3$_{\text{Tail}}$	0.69	0.82	18.32	0.58

Table 5.4: Fitted parameters of SISF of all classes of IW^{HB} for $\lambda = 0.60$ nm. Correlation coefficients are >0.99.

Region	τ_s (ps)	f_Q	τ_α (ps)	β_α	$f_{Q'}$	τ_l (ps)	β_l
IW^{HB}	0.24	0.50	3.49	0.91	0.45	43.00	0.62
IW-CO^{HB}	0.25	0.36	4.03	0.94	0.59	31.54	0.53
IW-Glyc^{HB}	0.22	0.33	3.90	0.99	0.64	30.64	0.54
IW-PO^{HB}	0.21	0.41	3.40	0.93	0.58	24.42	0.51
BW	0.10	0.90	3.54	0.94			

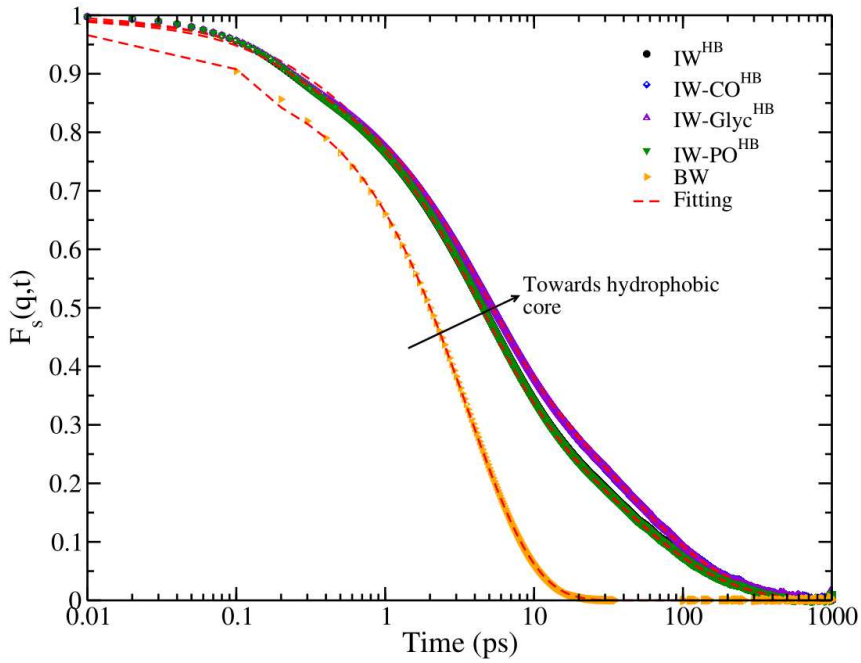

Figure 5.12: SISF for all classes of IW^{HB} at $\lambda = 0.60$ nm. IW-$Glyc^{HB}$ molecules buried deep in the hydrophobic core relax slowest.

A comparison of τ_α of lipids and IW^{HB} is shown in figure 5.14 a). τ_α of all classes of IW^{HB} and the respective lipid moieties decrease coherently from Carb to Glyc to P to N as reaching the outermost water like the BW. The ratio of the respective τ_α of lipid and IW^{HB} (figure 5.14 b) decreases following similar trend. Since the ratio ranges between $20 - 50$, τ_α of the lipid moieties and the respective IW^{HB} do not relax at the same time and not follow perfect coupling, but correlated by a scaling factor. To understand if the slowest dynamics of lipid and IW^{HB} are coupled or not, the slowest relaxation times of both lipids and IW^{HB} are plotted in figure 5.15 a). Since lipids do not have additional τ_l as the IW^{HB}, τ_α of lipids are compared with τ_l of IW^{HB}. τ_α of lipids become faster from Carb to Glyc to P to N as lipid moieties become more mobile towards lipid-water interface facing outermost water molecules. To understand the extent of correlations between the slowest dynamics of lipids and IW^{HB}, ratios of τ_l to τ_α are plotted in figure 5.15 b). Since the relaxations of different classes of IW^{HB} do not differ much, the ratios follow similar trend as the lipid head-groups. The ratio is closest to 1 for N facing outermost water molecules. More imperfect is the coupling, the ratio deviates more from 1. Since the lipid moieties are geometrically more constraint compared to the IW^{HB}, they move much slower compared to the IW^{HB} molecules and can not have perfectly coupled relaxations occurring at the same timescale as the confined IW^{HB} molecules. The long time relaxation obtained from SISF can also be characterized by the time SISF reaches value of $\frac{1}{e}$ [Michele *et al.*, 2011; Flenner and Szamel, 2013; Kim and Saito, 2013; Kuon *et al.*, 2017] which is associated with the escape of the molecules from their respective cages. Ratio for $\frac{1}{e}$ relaxation of lipids and IW^{HB} follow the same trend as obtained from the fitting of the SISF (figure 5.15 b)). Although the slowest relaxations between IW^{HB} and lipids are not perfectly coupled (the ratio is not equal to 1), they are closest to 1 for the outermost N among different head moieties. Similar trend is followed for the ratios from τ_s, τ_α and τ_l.

To understand the regional dynamics of a lipid membrane and its coupling with the IW^{HB}, both lipid components and IW^{HB} molecules are colormapped in terms of the fastest and slowest relaxation times and shown in figure 5.16. The fastest relaxation times, τ_s, decrease from the tail to the head groups of the lipids. τ_s of the lipid heads are strongly coupled with the nearest interface water as evident from the similar color maps (figure 5.16 a)). However, the slowest relaxation times, τ_α, of

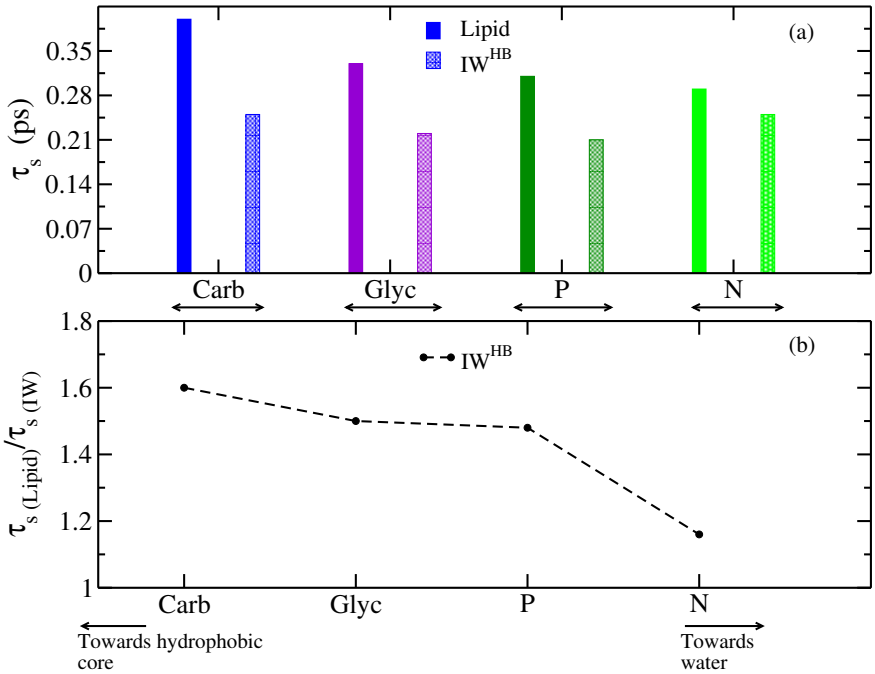

Figure 5.13: a) Shortest relaxation time scales, τ_s, are compared for the lipid head moieties and the IW^{HB} hydrogen bonded to the respective lipid heads. The values of τ_s are obtained in table 5.3 and 5.4. b) Ratio of τ_s of the lipid moieties and the IW^{HB}.

the lipids do not follow monotonic behavior from the tail to the head groups like their τ_s values. Instead the dynamics is fastest at both ends (head and tail) of the lipids and slowest in the middle (figure 5.16 b). The relaxation times of the lipid heads and the IW^{HB} confined close the head are correlated and therefore have close colormaps. The strong coupling in the fast relaxations as well as the correlations in the slow relaxations of the lipids and the confined IW^{HB} imply that the regional dynamics of different lipid head group moieties can be sensed by the respective IW^{HB} molecules. Therefore, any perturbation near lipid heads occurred by binding of a guest molecule should be monitored by the closest spatially resolved IW^{HB} dynamics. However the extents of correlations depend on the value of λ for which SISF is calculated. It has been observed that although the numerical values of the ratio of relaxation change with λ, the trend of coherent lipid and physically close IW^{HB} dynamics remains unaltered.

5.8 SUMMARY

In summary, the chapter investigates the complex multiple time-scale coupling between interface water and a lipid bilayer using all-atom molecular dynamics simulations at 308 K. Water molecules which reside in the interface layer located within ±3 Å away from the density of N head groups of the bilayer for a continuous time window of 100 ps are identified as IW^{HB}. The 100 ps time window is chosen for the confinement lifetime since the residence time of the IW^{HB} is $\sim$ 100 ps [Debnath *et al.*, 2010; Srivastava *et al.*, 2019a]. To understand the influence of the hydrogen bond on the coupling of the hydration layer and the bilayer these IW^{HB} are further classified based on their hydrogen bond partners, viz., P, Glyc, Carb and referred to as IW-PO^{HB}/$Glyc^{HB}$/CO^{HB} respectively. Previous experiments using SFG spectroscopy and molecular dynamics simulations reveal significance of similar chemically confined water molecules on the orientational or structural heterogeneity of interface water near cationic or anionic surfactant/lipid interfaces or zwitterionic phospholipids [Re *et al.*, 2014; Roy *et al.*, 2014; Ohto *et al.*, 2015; Inoue *et al.*, 2017; Cyran *et al.*,

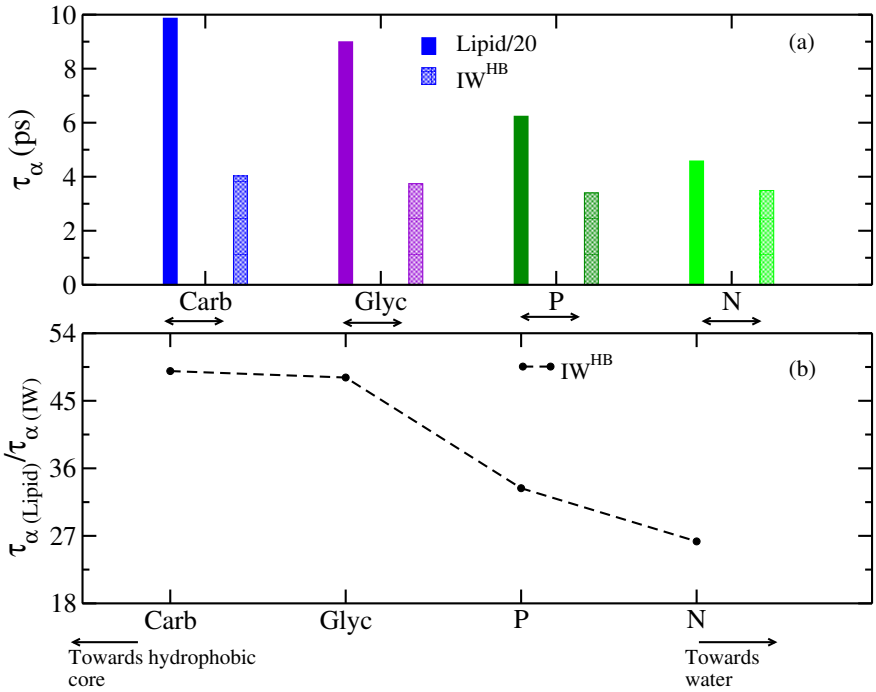

Figure 5.14: a) τ_α are compared for the lipid moieties and the IW. The values of τ_α are obtained from table 5.3 and 5.4. τ_α of lipids is divided by 20 for the clarity. b) Ratio of τ_α of the lipid moieties and the respective IW decreases as moving towards outer water.

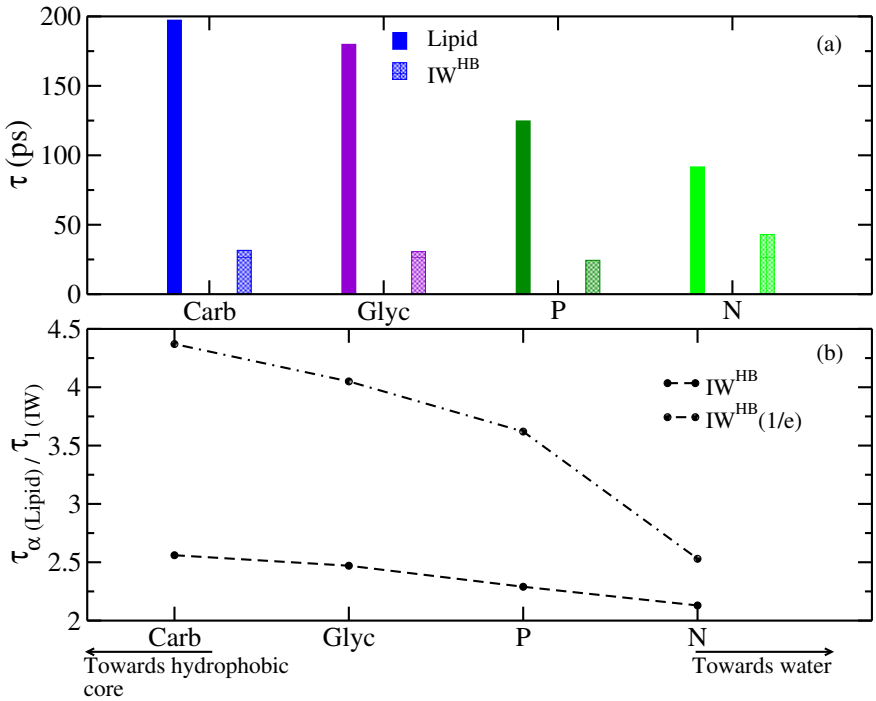

Figure 5.15: a) Slowest relaxation time scales are compared for lipid moieties (τ_α) and the IW^{HB} molecules (τ_l) hydrogen bonded to those lipid moieties. The time scales are obtained in table 5.3 and 5.4. b) Ratio of the slowest time-scales of the lipids and the IW obtained from SISF fitting and $\frac{1}{e}$ cut-off. τ_l of IW^{HB} obtained from $\frac{1}{e}$ is divided by 4.

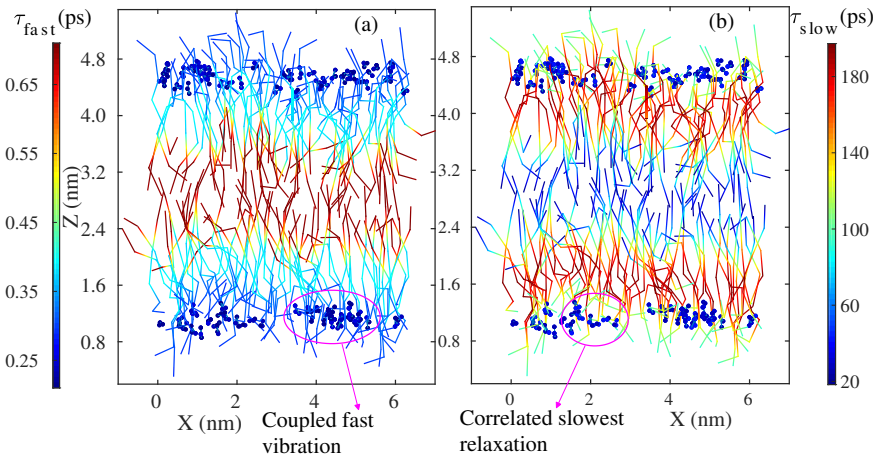

Figure 5.16: Colormap of a snapshot of a lipid bilayer and the IW^{HB} in terms of a) fast and b) relaxations for SISF calculated at $\lambda = 0.6$ nm for both DMPC and IW^{HB}. The fast relaxations are obtained from τ_s values in table 5.3 and 5.4. The slow relaxations for lipids and IW^{HB} are obtained from their τ_α (table 5.3) and τ_l (table 5.4) values respectively.

2018]. The retardation factors of the lipid head moieties decrease from the deeper hydrophobic side to the outermost water side.

The previous chapter discusses that the slow relaxations of IW^{HB} is originated from dynamical heterogeneity even at room temperature [Srivastava *et al.*, 2019a]. As the lipid components approach from the head to the tail lying on the midplane of the hydrophobic core, the van Hove correlation functions approach Gaussianity. The Gaussian distribution of the end tail beads are attributed to their flexible and less constraint mobility in the absence of IW^{HB}. On the other side, the distribution is non-Gaussian at the end head beads of lipids to which IW^{HB} molecules reside closest. Since the lipid components move much slower compared to the IW^{HB} molecules as evident from their MSD, the underlying distribution of lipids should be more non-Gaussian compared to the IW^{HB}. To understand the opposite trend of IW^{HB} and lipids in van Hove correlation functions, distribution of logarithm of displacements of the IW^{HB} and the P lipid heads are calculated. With time, the IW^{HB} molecules develop a bimodal nature which is a characteristic of intermittent behavior leading to dynamical heterogeneity. The time by which the IW^{HB} follow Fickian behavior are still intermittent and non-Gaussian in nature. This clearly confirms that MSD_{XY} is not an appropriate measure for deciphering underlying dynamics. The IW^{HB} molecules do not reach Gaussianity even at a time-scale 7 times slower than the time of linear behavior in MSD. The IW^{HB} molecule vibrates for sometime in a cage or segment formed by the hydrogen bonds to a lipid head followed by a translational jump to another segment where it is hydrogen bonded to another lipid head. Although the IW^{HB} molecule jumps from one segment to the other segment, the hydrogen bonded lipid molecule does not jump coherently with the IW^{HB} not resulting in a perfect coupling between them. The decoupling in individual lipid-IW^{HB} dynamics and the intermittency in the IW^{HB} result in dynamical heterogeneity in the IW^{HB}. Intermittency is known to be present in supercooled bulk water due to fluctuations in high density 5 coordinated and low density 4 coordinated water molecules [Jana and Bagchi, 2009]. Although lipid and IW^{HB} molecules do not relax at the same time scale, dynamics of IW^{HB} molecules are significantly influenced by the regional dynamics of lipids.

Self intermediate scattering functions of the lipid moieties exhibit two time-scales: fast ballistic motion in a cage and long relaxations of the cage. Interestingly, IW^{HB} molecules show an additional long time scale with an intermediate hopping time scale. Such three well separated time-scales are found earlier for water in the vicinity of protein due to the fluctuations in protein structure [Marzio *et al.*, 2016]. On comparing both fast and slow relaxations of IW^{HB} with that of the lipid moieties,

fast relaxations of both IW^{HB} and respective lipids are found to be coupled as they vibrate together in the local cage formed either by physically close neighboring molecules or connected by hydrogen bonds. The fast relaxations of lipid moieties in the respective cages are slower from the head to the tail beads approaching the bilayer midplane. However, the slow relaxations of the lipid components are more complex in nature and do not follow any monotonic change from the head to the tail. Instead, the slow relaxations are faster at the two ends of a chain compared to the relaxations of beads at the middle. Ratio of slow relaxations of the lipids and the IW^{HB} is closest to 1 near the outermost N head-group among the remaining moieties. This is because N heads are most mobile at the lipid head-water interface with faster relaxation time scales and different classes of IW^{HB} have similar relaxation time scales since all of them reside closest to N head-groups. Thus our analysis sheds light on quantification of coupling between lipid and IW^{HB} multiple time-scale relaxations at a fluid phase. Very similar coupling has been found for protein-water interface using component wise molecular dynamics study [Wohlfromm and Vogel, 2019]. Our results explain the origin of dynamical heterogeneity in IW^{HB} through intermittency due to the hydrogen bond breaking and formation with different lipid moieties in the interface. Our calculations show that the IW^{HB} relaxations can not influence the dynamics of lipids occurring on different time-scales, but regional dynamics of lipids can be reflected in the regional dynamics of IW^{HB}. This strongly supports the idea that IW^{HB} can act as a sensor for capturing the regional complex dynamics of lipids which is not easy to access through experiments. At the same time, our findings pave the way to a better understanding on membrane-protein or membrane-drug interactions through water dynamics in future. The analysis will have implications towards IW^{HB} dynamics used as a finer tool to monitor the dynamics of lipids generating skeleton fences, molecular recognition, rafts and so on [Munro, 2003; Lingwood and Simons, 2010; He *et al.*, 2016].